Available online at www.sciencedirect.com
ScienceDirect
Polyhedron 26 (2007) 2810–2816
POLYHEDRON
www.elsevier.com/locate/poly

Synthesis and characterization of near-infrared absorption tin octabutoxy naphthalocyanines

Cheolbeom Bae [a], Gwanghoon Kwag [a,*], Malcolm E. Kenney [b]

[a] R & BD Center, Korea Kumho Petrochemical Co., Ltd., P.O. Box 64, Yuseong, Taejeon 305-600, Republic of Korea
[b] Department of Chemistry, Case Western Reserve University, Cleveland, OH 44106, USA

Received 11 December 2006; accepted 22 January 2007
Available online 7 February 2007

Abstract

Synthesis and characterization of a series of tin octabutoxy naphthalocyanines are presented, which show near infrared absorptions (900–930 nm) with high extinction coefficients (*ca.* 1×10^5 M^{-1} cm^{-1}). The position of the Q-band is more red-shifted with the heavier halogen, which corresponds to the HOMO–LUMO gaps calculated with density functional theory (0.932, 0.911, 0.905, 0.893 eV). The interaction with $SnNc(OBu)_8Br_2$ and C_{60} moves the Q-band further to the infrared region (928 nm). In ^{119}Sn NMR, the upfield shift (−120 ppm) of $SnNc(OBu)_8I_2$ represents a relatively electron-rich environment at the tin nucleus, and the ^{119}Sn-resonance (237 ppm) of $SnNc(OBu)_8F_2$ is different from the other halides, where ^{119}Sn–^{19}F coupling, a triplet splitting (1:2:1), was observed with 1820 Hz coupling constant. In the optimized structures obtained with BLYP, the distortion angles vary from F to I (N–Sn–N angles 178.8°, 173.1°). The tin naphthalocyanine with the heavy halide ligand becomes more concave, and the Sn–X bond is located at a longer distance out of ring. The difference of the two axial bonds varies significantly from 0.003 to 0.104 Å with the change of the axial ligands from F to I. The distorted shape is larger in the order I > Br > Cl > F with increase of the atomic size (1.33, 1.15, 0.99, 0.71 Å, respectively) and decrease of electronegativity (2.21, 2.74, 2.83, 4.10, respectively). $SnNc(OMe)_8X_2$ has an electric dipole moment perpendicular to the naphthalocyanine plane, and the magnitudes are, 0.81, 0.50, 0.35 and 0.01 for F, Cl, Br and I, respectively. The transition dipole moment lies in the naphthalocyanine plane along the *x*- or *y*-axis perpendicular to the permanent dipole moment in the *z*-axis, which indicates a $\pi \rightarrow \pi^*$ ligand–ligand transition. The energies of the molecular orbitals which are mainly contributed to by the naphthalocyanine ring, including the HOMO and LUMO, are slightly changed as the axial ligands change from F to I.

Keywords: Tin octabutoxy naphthalocyanine; Near infrared absorption; Q-band; Molecular orbitals

1. Introduction

Naphthalocyanines, extended conjugated macrocycles with high chemical and thermal stabilities, have been studied in many application areas for molecular electronics, non-linear optics, optical data storage, sensors, electrochromic devices, solar cells, electrocatalytic systems and photodynamic therapy [1–4]. As near infrared absorption (NIR) materials, napthalocyanine has chromophoric and low-band-gap properties, and the electronic structure of napthalocyanine can be tuned by the peripheral substitution of the ring, and the kind of central metal and axial ligands [5,6].

Our aim is to prepare a series of tin naphthalocyanine halides showing near infrared absorption and to understand their electronic and molecular structures.

2. Experimental

2.1. Materials

The tin halides (SnF_2, $SnCl_2 \cdot 2H_2O$, $SnBr_2$, SnI_2) and 1,4-dibutoxy-2,3-naphthalenedicarbonitrile were purchased

* Corresponding author. Tel.: +82 42 865 8698; fax: +82 42 862 5651.
E-mail address: gkwag@kkpc.com (G. Kwag).

0277-5387/$ - see front matter © 2007 Elsevier Ltd. All rights reserved.
doi:10.1016/j.poly.2007.01.045

from Aldrich Chemical. Polystyrene beads used in gel permeation column chromatography were obtained from Bio-Rad Laboratories.

2.2. Spectroscopies

The electronic spectra were obtained with a UV–Vis–NIR spectrophotometer (JASCO). ^{1}H, ^{19}F, ^{119}Sn NMR spectra were recorded with Varian XL-200, Gemini 300 and Bruker MSL-400 spectrometers. The low- and high-resolution fast-atom-bombardment (LR FAB and HR FAB) mass spectra were obtained from either the Midwest Center for Mass Spectrometry (University of Nebraska-Lincoln, NE) or Washington University Resource for Biomedical and Bio-organic Mass Spectrometry. The elemental analyses were carried out by a commercial laboratory (Galbraith Laboratories, Knoxville, TN).

2.3. Calculation

Geometry optimizations of $SnNc(OMe)_8X_2$ (X = F, Cl, Br and I) were carried out without any symmetry constraints. We introduced a methoxy group instead of the butoxy group for relatively insignificant rotational conformations of the butoxy group. Our calculations were based on the density functional theory at the generalized gradient approximation level, BLYP functional [7]. Energy-adjusted relativistic effective core potentials were used for Br, I and the central Sn atom [8]. Double numerical plus polarization basis sets were used for the C, N, O, H, F, Cl atoms and the valence electrons for Br, I and Sn [9]. All calculations were performed using the DMOL^3 program [10]. In order to aid the interpretation of the absorption spectrum, spectroscopic calculations were performed at the BLYP-optimized geometries within the ZINDO approximation implemented in the VAMP program [11,12].

2.4. Synthesis

$H_2Nc(OBu)_8$. $H_2Nc(OBu)_8$ was prepared according to the literature [13].

$SnNc(OBu)_8F_2$. Under N_2, a mixture of $H_2Nc(OBu)_8$ (40 mg, 0.031 mmol), SnF_2 (220 mg, 1.40 mmol) and dry 2-ethylpyridine (5 mL) was refluxed for 100 min, cooled and evaporated to dryness with a rotary evaporator (~30 °C, ~1 Torr). The solid was chromatographed (Bio-Beads S-X4, 1.7 × 30 cm; toluene), dried (~60 Torr, ~60 °C) and weighed (12 mg, 0.0083 mmol, 27%). IR (Nujol): 558 (Sn–F) cm^{-1}. ^{1}H NMR (300 MHz, C_6D_6): δ 9.17 (m, 1,4-Nc H), 7.67 (m, 2,3-Nc H), 5.25 (t, α-CH_2), 2.30 (m, β-CH_2), 1.66 (m, γ-CH_2), 1.05 (t, CH_3). ^{13}C NMR (75 MHz, C_6D_6): δ 152.1 (s), 149.4 (s), 131.8 (s), 128 (s), 125.0 (s), 77.8 (s), 33.4 (s), 19.9 (s), 14.5 (s). ^{119}Sn NMR (75 MHz, C_6D_6): δ 237 J^1(Sn–F) = 1820.2 Hz (24.4 ppm). ^{19}F NMR (376 MHz, C_6D_6): δ −126. MS-FD, *m*/*z*: calc. for $C_{80}H_{88}N_8O_8F_2Sn$ $(M)^+$, 1446; found 1446. MS-HRFAB exact mass, *m*/*z*: calc. for $C_{80}H_{88}N_8O_8F_2Sn^{116}$ $(M)^+$, 1442.5711; found 1442.5713, 1442.5663. UV–Vis (λ_{max} (nm), ε ($M^{-1}\,cm^{-1}$)) (CH_2Cl_2): 906, 1.1×10^5. The compound is dark brown. It is soluble in CH_2Cl_2, toluene, and slightly soluble in hexane. It is insoluble in CH_3OH and H_2O.

$SnNc(OBu)_8Cl_2$. Under N_2, a mixture of $H_2Nc(OBu)_8$ (58 mg, 0.045 mmol) and $SnCl_2 \cdot 2H_2O$ (300 mg, 1.33 mmol) was refluxed in dry dimethylformamide (5 mL) for 4 h, cooled and evaporated to dryness with a rotary evaporator (~30 °C, ~1 Torr). The solid was extracted with toluene (5 mL), and the extract was evaporated to dryness with a rotary evaporator (~30 °C, ~1 Torr). The solid thus obtained was chromatographed (Bio-Beads S-X4, 1.5 × 20 cm; toluene), dried (~60 °C, ~60 Torr) and weighed (20 mg, 0.014 mmol, 31%). ^{1}H NMR (300 MHz, C_6D_6): δ 9.14 (m, 1,4-Nc H), 7.67 (m, 2,3-Nc H), 5.25 (t, α-CH_2), 2.24 (m, β-CH_2), 1.62 (m, γ-CH_2), 1.01 (t, CH_3). ^{13}C NMR (75 MHz, C_6D_6): δ 152.4 (s), 148.8 (s), 132.0 (s), 128 (s), 125.0 (s), 122.9 (s), 77.9 (s), 33.3 (s), 19.8 (s), 14.6 (s). ^{119}Sn NMR (75 MHz, C_6D_6): δ 266. MS-FD, *m*/*z*: calc. for $C_{80}H_{88}N_8O_8Cl_2Sn$ $(M)^+$, 1479; found 1478. MS-HRFAB exact mass, *m*/*z*: calc. for $C_{80}H_{88}N_8O_8Cl_2Sn^{116}$ $(M)^+$, 1474.5119; found 1474.5064, 1474.5087. UV–Vis (λ_{max} (nm), ε ($M^{-1}\,cm^{-1}$)) (CH_2Cl_2): 923, 1.0×10^5. The compound is dark brown. It is soluble in CH_2Cl_2, toluene, benzene, and slightly soluble in hexane. It is insoluble in CH_3OH and H_2O.

$SnNc(OBu)_8Br_2$. Under N_2, a mixture of $H_2Nc(OBu)_8$ (45 mg, 0.035 mmol), $SnBr_2$ (190 mg, 0.682 mmol), dry 2-ethylpyridine (0.3 mL) and dry xylenes (3 mL) was refluxed for 3 h, and evaporated to dryness with a rotary evaporator (~30 °C, ~1 Torr). The solid was extracted with toluene (5 mL), and the extract was evaporated to dryness with a rotary evaporator (~30 °C, ~1 Torr). The resulting solid was chromatographed (Bio-Beads S-X4, 1.5 × 20 cm; toluene), dried (~60 Torr, ~60 °C) and weighed (19 mg, 0.012 mmol, 34%). ^{1}H NMR (300 MHz, C_6D_6): δ 9.13 (m, 1,4-Nc H), 7.67 (m, 2,3-Nc H), 5.25 (t, α-CH_2), 2.21 (m, β-CH_2), 1.60 (m, γ-CH_2), 0.99 (t, CH_3). ^{13}C NMR (75 MHz, C_6D_6): δ 152.5 (s), 148.7 (s), 132.1 (s), 128 (s), 125.0 (s), 122.7 (s), 77.92 (s), 33.27 (s), 19.84 (s), 14.40 (s). ^{119}Sn NMR (75 MHz, C_6D_6): δ 142. MS-FD, *m*/*z*: calc. for $C_{80}H_{88}N_8O_8Br_2Sn$ $(M)^+$, 1568; found, 1568. MS-HRFAB exact mass, *m*/*z*: calc. for $C_{80}H_{88}N_8O_8Sn^{120}$ $(M-2Br)^+$, 1408.5747; found, 1408.5730, 1408.5748. UV–Vis (λ_{max} (nm), ε ($M^{-1}\,cm^{-1}$)) (CH_2Cl_2): 924, 1.2×10^5. The compound is dark brown. It is soluble in CH_2Cl_2, toluene, and slightly soluble in hexane. It is insoluble in CH_3OH and H_2O.

$SnNc(OBu)_8I_2$. Under N_2, a mixture composed of $H_2Nc(OBu)_8$ (50 mg, 0.039 mmol), SnI_2 (99.9%, 280 mg, 0.752 mmol), dry 2-ethylpyridine (0.3 mL) and xylenes (3 mL) was refluxed for 4 h, cooled and evaporated to dryness with a rotary evaporator (~30 °C, ~1 Torr). The solid was extracted with toluene (5 mL) and the extracted was evaporated to dryness with a rotary evaporator (~30 °C, ~1 Torr). The solid thus obtained was chromatographed

(Bio-Beads S-X4, 1.5 × 20 cm; toluene), dried (~60 °C, ~60 Torr) and weighed (36 mg, 0.022, 56%). ^{1}H NMR (300 MHz, C_6D_6): δ 9.12 (m, 1,4-Nc H), 7.67 (m, 2,3-Nc H), 5.27 (t, α-CH_2), 2.18 (m, β-CH_2), 1.56 (m, γ-CH_2), 0.96 (t, CH_3). ^{13}C NMR (75 MHz, C_6D_6): δ 52.6 (s), 148.7 (s), 131.2 (s), 128 (s), 125.1 (s), 122.5 (s), 78.2 (s), 33.2 (s), 19.8 (s), 14.4 (s). ^{119}Sn NMR (75 MHz, C_6D_6): δ-120. *Anal.* Calc. for $C_{80}H_{88}N_8O_8I_2Sn$: C, 57.80; H, 5.34; I, 15.27. Found: C, 57.43; H, 5.47; I, 15.37%. MS-FD, *m*/*z*: calc. for $C_{80}H_{88}N_8O_8I_2Sn$ $(M)^+$, 1662; found 1662. UV–Vis (λ_{max} (nm), ε (M^{-1} cm^{-1})) (CH_2Cl_2): 926, 1.0×10^5. The compound is dark brown. It is soluble in toluene, CH_2Cl_2, and slightly soluble in hexane. It is insoluble in CH_3OH and H_2O.

SnNc(OBu)$_8$(OSi(n-C$_6$H$_{13}$)$_3$)$_2$. Under N_2, a mixture composed of $SnNc(OBu)_8Br_2$ (30 mg, 0.019 mmol) and a mixture of $HOSi(n\text{-}C_6H_{13})_3$ (100 μL, 0.26 mmol), $NaOCH_3$ (10 mg, 0.19 mmol) and dry toluene (5 mL), which had previously been refluxed for 1 h, was refluxed for 2 h and evaporated to dryness with a rotary evaporator (~40 °C, ~1 Torr). The solid was washed with ethanol (50 mL), dried (~25 °C, ~60 Torr), chromatographed (Bio-Beads S-X4, 1.7 × 25 cm; toluene), dried (~60 °C, ~60 Torr) and weighed (22 mg, 0.011 mmol, 58%). M.p.: 156–8 °C. ^{1}H NMR (300 MHz, C_6D_6): δ 9.20 (m, 1,4-Nc H), 7.67 (m, 2,3-Nc H), 5.60 (t, C_4H_9 α-CH_2), 2.45 (m, C_4H_9 β-CH_2), 1.78 (m, C_4H_9 γ-CH_2), 1.11 (t, C_4H_9 CH_3), 0.67 (m, C_6H_{13} ε-CH_2), 0.41 (t, C_6H_{13} CH_3), 0.39 (m, C_6H_{13}γ- and δ-CH_2), −0.14 (m, C_6H_{13} β-CH_2), −1.11 (m, C_6H_{13}α-CH_2). The compound is dark brown. It is soluble in CH_2Cl_2, toluene and hexane. It is insoluble in CH_3OH and H_2O.

3. Results and discussion

3.1. Synthesis

The synthetic routes for the preparation of $SnNc(OBu)_8X_2$ (X = F, Cl, Br, I) were a template cyclization and a metal insertion. Lithium butoxide catalyzed and templated cyclization of 1,4-dibutoxy-2,3-napthalenedicarbonitrile, and the lithiated naphthalocyanine was converted to the metal-free naphthalocyanine in an acidic work-up step. The halo tin naphthalocyanines were obtained by reactions with the metal-free octabutoxy naphthalocyanine and the corresponding metal halides. Here, octabutoxy groups render good solubility in organic solvents such as toluene or dichloromethane. It is interesting that both SnX_2 and SnX_4 reacted well for tin insertion except SnF_4, and SnX_2 showed higher reactivity than SnX_4. The halide ligands can be exchanged by the highly soluble trihexylsiloxy. $SnNc(OBu)_8(OSiHx_3)_2$ was made by the ligand exchange reaction of $SnNc(OBu)_8Br_2$ and $NaOSiHx_3$ in toluene. The trihexylsiloxy ligands provide good solubility in non-polar solvents such as *n*-hexane, which is important in high concentration applications for recording disks.

3.2. NMR spectra

In the proton NMR resonances of $SnNc(OBu)_8X_2$ (X = F, Cl, Br, I, $OSi(n\text{-}C_6H_{13})_3$), the α- and β-methylene resonances of the butoxy groups are in the ranges δ 5.2–5.3 and 2.2–2.3 ppm, respectively, for the halides and δ 5.60 and 2.45 ppm for $OSi(n\text{-}C_6H_{13})_3$, as shown in Table 1. This suggests that the shieldings of α- and β-protons of the tin halo naphthalocyanines arising from ring-current effects are similar to one another, but are different from those of the trihexylsiloxy naphthalocyanine. ^{119}Sn NMR spectra, a very sensitive technique for determination of the coordination environment of the tin atom, are useful to study the structures of tin octabutoxy naphthalocyanine halides [14]. Of the 10 naturally occurring isotopes of tin, only ^{119}Sn (I = 1/2, 8.6% abundance) is a practical choice due to its slightly higher abundance and its greater sensitivity to NMR detection. ^{119}Sn NMR resonances of $SnNc(OBu)_8X_2$ are seen in Fig. 1. The trend in chemical shifts is not linear with respect to the electronegativity of the ligands. A downfield shift appears from F to Cl and then a linear upfield shift occurs from Cl to I. Simply explained, the ^{119}Sn chemical shifts would depend on the properties of the axial ligands and directly reflect the electron density at the tin nucleus. The upfield shifts of $SnNc(OBu)_8I_2$ represent a relative electron-rich environment at the tin nucleus. $SnNc(OBu)_8F_2$ exhibits a NMR spectrum different from the other halides. For the first-row element F the σ-bonding effect dominates, but for the other halides the π-bonding effect should be considered as well. These halides possess weak participation of Sn–X p_π–p_π bonding. The observed Sn–F coupling for $SnNc(OBu)_8F_2$, a triplet splitting (1:2:1), is 1820 Hz, which results from the ^{119}Sn–^{19}F *J* coupling. The ^{19}F NMR was taken to study the structure of $SnNc(OBu)_8F_2$, and $CFCl_3$ is used as the chemical shift reference [15]. A strong intense peak with two pairs of coupling peaks at −126 ppm was found. The two doublets correspond to ^{117}Sn and ^{119}Sn spin couplings to axial fluorines.

3.3. UV–Vis–NIR spectra

The tin octabutoxy naphthalocyanine halides have very strong bands in the near infrared region (>900 nm), as shown in Fig. 2. These bands are considerably red shifted as compared to the spectra of a simple naphthalocyanine

Table 1
^{1}H NMR resonances of octabutoxy tin naphthalocyanines ($SnNc(OBu)_8X_2$) in C_6D_6

X	F	Cl	Br	I	$OSi(n\text{-}C_6H_{13})_3$
α-CH_2	5.25	5.25	5.25	5.27	5.60
β-CH_2	2.30	2.24	2.21	2.18	2.45
γ-CH_2	1.66	1.62	1.60	1.56	1.78
δ-CH_2	1.05	1.01	0.99	0.96	1.11
2,3-Nc H	7.67	7.67	7.67	7.67	7.67
1,4-Nc H	9.17	9.14	9.13	9.12	9.20

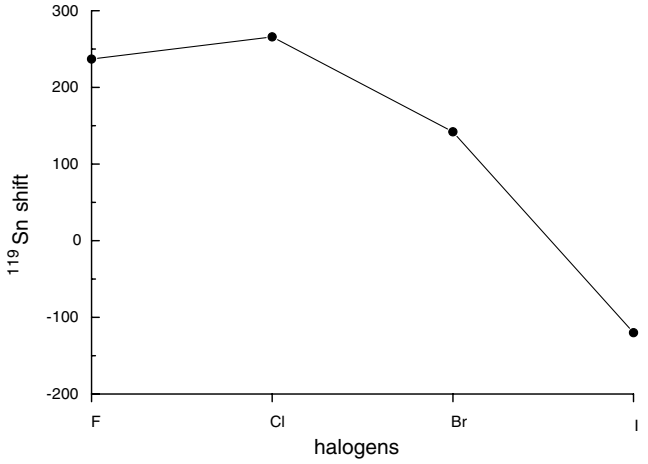

Fig. 1. Plot of the ^{119}Sn chemical shift of $SnNc(OBu)_8X_2$ vs. halogen.

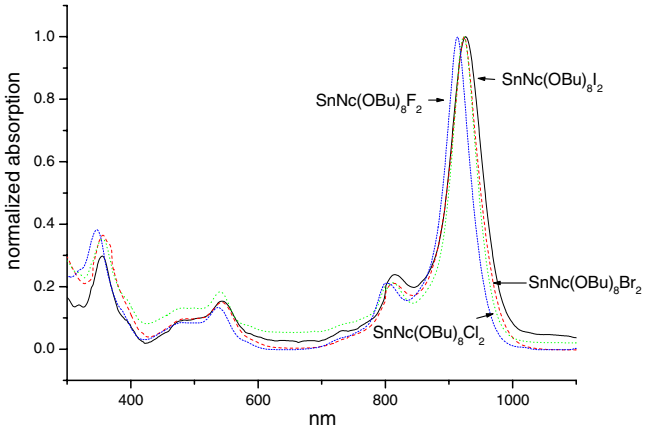

Fig. 2. UV–Vis spectra of $SnNc(OBu)_8X_2$ (X = F, Cl, Br, I).

(780 nm), octabutoxy naphthalocyanine (862 nm) or $PdNc(OBu)_8$ (892 nm). This result shows tin and halides (F, Cl, Br and I) can significantly influence the red shift of the Q-bands. The position of the Q-band in the series $SnNc(OBu)_8F_2$ (906 nm) to $SnNc(OBu)_8I_2$ (926 nm) is more shifted the heavier the halogen. The UV–Vis absorption data of a mixture of $SnNc(OBu)_8Br_2$ and C_{60} was obtained in CH_2Cl_2, as shown in Fig. 3. The extended aromatic surface of the naphthalocyanine will interact with C_{60} by π–π interactions. The Q band of $SnNc(OBu)_8Br_2$ was a little red-shifted to 928 nm (*ca.* 4 nm), and a peak at 330 nm appeared, partly attributed to C_{60}. The small red-shift would be the result of complexation of $SnNc(OBu)_8Br_2$ and C_{60}, lowering the π–π^* transition energy of the tin naphthalocyanine [16].

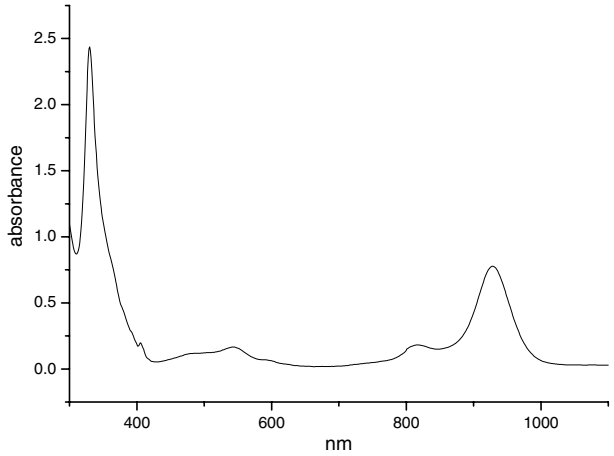

Fig. 3. UV–Vis absorption change of $SnNc(OBu)_8Br_2$ resulting from binding C_{60}.

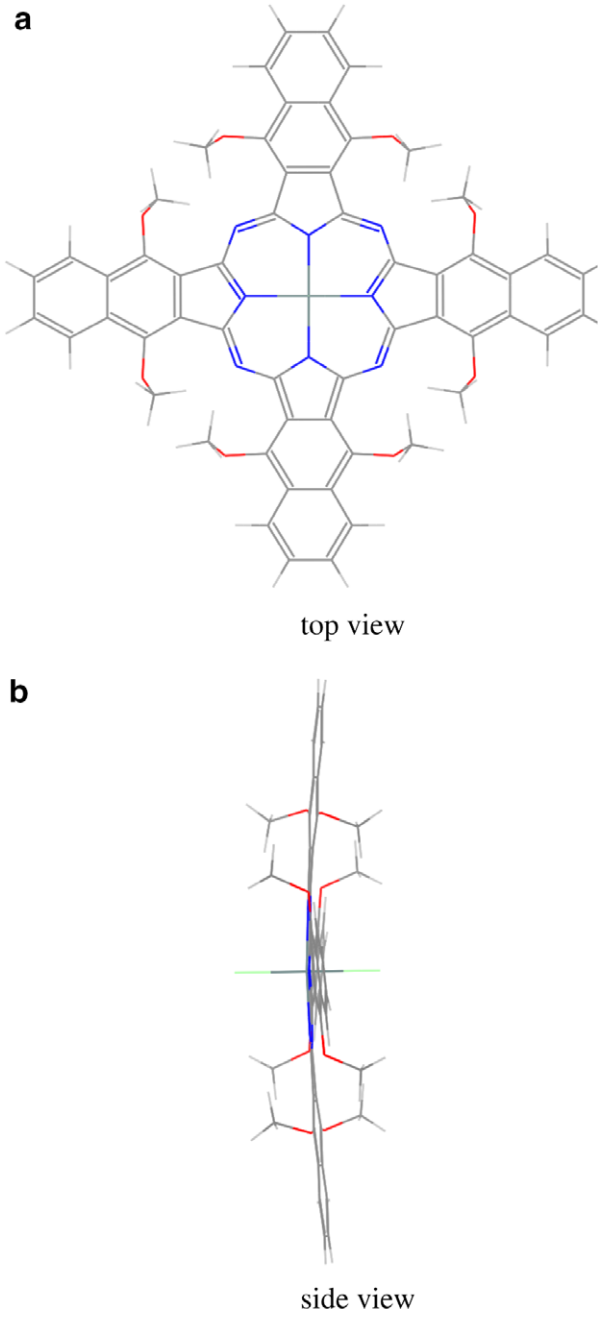

Fig. 4. The optimized molecular structure of $SnNc(OMe)_8X_2$, and the optimized bond lengths, distances and angles defined in the figure are compiled in Table 2. (a) Top view (b) side view.

Table 2
The optimized geometric parameters in the optimized structure of Fig. 4

X	Sn–X (Å)	Sn–X′ (Å)	Δ (Å)	Sn–N (Å)	h (Å)	N–Sn–N (°)	C_2–Sn–C_{20} (°)	C_3–Sn–C_{21} (°)
F	2.014	2.017	0.003	2.101	0.022	178.8	172.8	174.4
Cl	2.486	2.530	0.044	2.107	0.075	175.9	172.0	173.7
Br	2.667	2.728	0.061	2.108	0.092	175.0	171.7	173.4
I	2.900	3.004	0.104	2.110	0.127	173.1	170.4	172.2

Table 3
Experimental and calculated absorption wavelengths at the ZINDO using the BLYP-optimized geometries

X	λ_{max}^{EXP} (nm)	λ_{max}^{ZINDO} (nm)	Δ(LUMO–HOMO)^{BLYP} (nm (eV))
F	906	827.6	1330(0.932)
Cl	923	833.6	1361(0.911)
Br	924	836.4	1370(0.905)
I	926	841.0	1388(0.893)

3.4. Theoretical calculation

For a better understanding the spectroscopic results, a theoretical calculation was carried out using density functional theory at the generalized gradient approximation level, BLYP functional. Geometry optimizations of $SnNc(OMe)_8X_2$ (X = F, Cl, Br and I) were carried out without any symmetry constraints. We introduced a methoxy group instead of the butoxy group for relatively insignificant rotational conformations of OC_4H_9. The direction of methoxy on naphthalocyanine changes the planarity of naphthalocyanine, and results in several isomers. In the most stable isomer, two adjacent methoxy groups are locate in opposite directions to each other to reduce steric repulsion. In the case where all eight methoxy groups are located on the same upside or downside of the naphthalocyanine plane, the isomers have higher energies than the most stable isomers by *ca.* 20 kcal/mol. The optimized structure of the most stable $SnNc(OMe)_8X_2$ is shown in Fig. 4, and the optimized bond lengths, distances and angles defined in the figure are compiled in Table 2. As two methoxy groups on an isobenzoindole moiety are located on the upside and downside of the naphthalocyanine plane, the four isobenzoindole moieties of naphthalocyanine spread outwards in a propeller-shaped distortion. The increase of steric repulsion between the oxygen lone pairs of the facing alkoxy ligands is thought to lead to the distortion. Two C_2–Sn–C_{20} and C_3–Sn–C_{21} angles represent the degree of both naphthalocyanine planarity and distortion of isobenzoindole.[1] From F to I, the distortion of isobenzoindole increases with a slight increase of the difference between the C_2–Sn–C_{20} and C_3–Sn–C_{21} angles, and the naphthalocyanine plane becomes more concave. The deformation of the naphthalocyanine plane is accompanied by a displacement of the Sn atom out of the plane. The side view in Fig. 4b shows that the Sn atom lies above the naphthalocyanine plane. The distance, h, is defined as the out-of-plane distance of the Sn atom from the center of the naphthalocyanine plane. As the axial ligands change from F to I, the distance h varies from 0.022 to 0.127 Å. The angle N–Sn–N defined as the average bond angle between the Sn and the N atoms, also indicates the out-of-plane nature of the Sn atom. As the N–Sn–N angles decrease from F to I, the naphthalocyanine ring becomes a deep saucer-shape. The distorted shape (Sn–N angle 178.8°, 175.9°, 175.0°, 173.1°) is larger in the order of I > Br > Cl > F, with increase of the atomic size (1.33, 1.15, 0.99, 0.71 Å, respectively) and decrease of electronegativity (2.21, 2.74, 2.83, 4.10, respectively).[2] The non-planarity of the naphthalocyanine generates the two different axial-bond lengths. The axial Sn–X bond located inside of the concave, elongates more than the other axial Sn–X bond. The difference of the two axial bonds varies significantly from 0.003 to 0.104 Å with the change of the axial ligands from F to I. $SnNc(OMe)_8X_2$ has an electric dipole moment perpendicular to the naphthalocyanine plane. The electric dipole moment of $SnNc(OMe)_8X_2$ points from the halide located on the inside of the concave to the central Sn atom along the z-axis, and the magnitudes are, 0.81, 0.50, 0.35 and 0.01 for F, Cl, Br and I, respectively. A strong electronegative halide shows a high magnitude of dipole moment and presents a permanent dipole moment along the z-axis which could be advantageously used to achieve molecular orientation and poling. In order to aid the interpretation of the absorption spectra, spectroscopic calculations were performed at the BLYP-optimized geometries within the ZINDO approximation implemented in the VAMP program [11,12]. The calculated absorption λ_{max} values are also listed in Table 3. The calculations have not taken the solution environment into account, which may affect the electronic transitions and geometry. Compared with the experimental data, the calculated λ_{max} values are red-shifted by about 85 nm under the average error of 9%. In spite of the λ_{max} difference, good qualitative agreement is found between the calculations and experiments. The HOMO and LUMO gap decreases from F to I. The HOMO and LUMO at the BLYP level of theory are depicted in Fig. 5. The HOMO, filled π-type orbital, has a highly symmetric flowerlike structure with a big hole at the Sn atom, and presents nodes at every nitrogen atom of the naphthalocyanine. The LUMO, an empty π^*-type orbital, was doubly degenerate with a twofold spatial

[1] See supporting information Figure S1.

[2] http://periodic.lanl.govurlhttp://periodic.lanl.gov/default.htm.

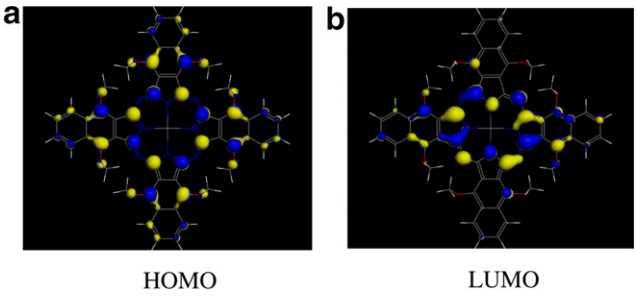

Fig. 5. The HOMO–LUMO at the BLYP level of theory (a) HOMO (b) LUMO.

symmetry. The LUMO + 1 has the same spatial structure but is rotated by 90° from the LUMO. The LUMO or LUMO + 1 consists mainly of π-orbitals, delocalized over the isobenzoindole moieties along the *x*- or *y*-axis. Disregarding the asymmetry introduced by the methoxy ligands, distortion and non-planarity, the symmetry of the HOMO and LUMO/LUMO + 1 are a_{2u} and e_g, respectively. The calculated absorption λ_{max} corresponds to the excitation from the HOMO(a_{1u}) to the LUMO or LUMO + 1(e_g). The transition dipole moment lies in the naphthalocyanine plane along the *x*- or *y*-axis, perpendicular to the permanent dipole moment in the *z*-axis, which also indicates λ_{max} results from a ligand–ligand transition ($\pi \rightarrow \pi^*$). The correlation diagram shows the molecular orbitals of $SnNc(OMe)_8X_2$ (X = F, Cl, Br and I) and their orbital energies in Fig. 6. The 4d subshell orbital of Sn is expected to be filled and is deep enough to form almost pure molecular orbitals. The overlap between the valence orbitals of Sn and the halogen ligands play a significant role in bonding, and the molecular orbitals mainly composed of the valence p orbitals of axial ligands are located under the HOMO. Moving down a column of the periodic table, valence s and p orbitals of halogen ligands are more extended with higher energy. The orbital energies of molecular orbitals mainly contributed from the valence p orbitals of axial ligands rise sharply as the axial ligands change from F to I. In the case of $SnNc(OMe)_8I_2$, the molecular orbitals mainly composed of p_x or p_y orbitals of the axial ligands are underneath the HOMO. The atomic charges on the axial ligands are expected to be distributed into the molecular orbital which is mainly composed of valence

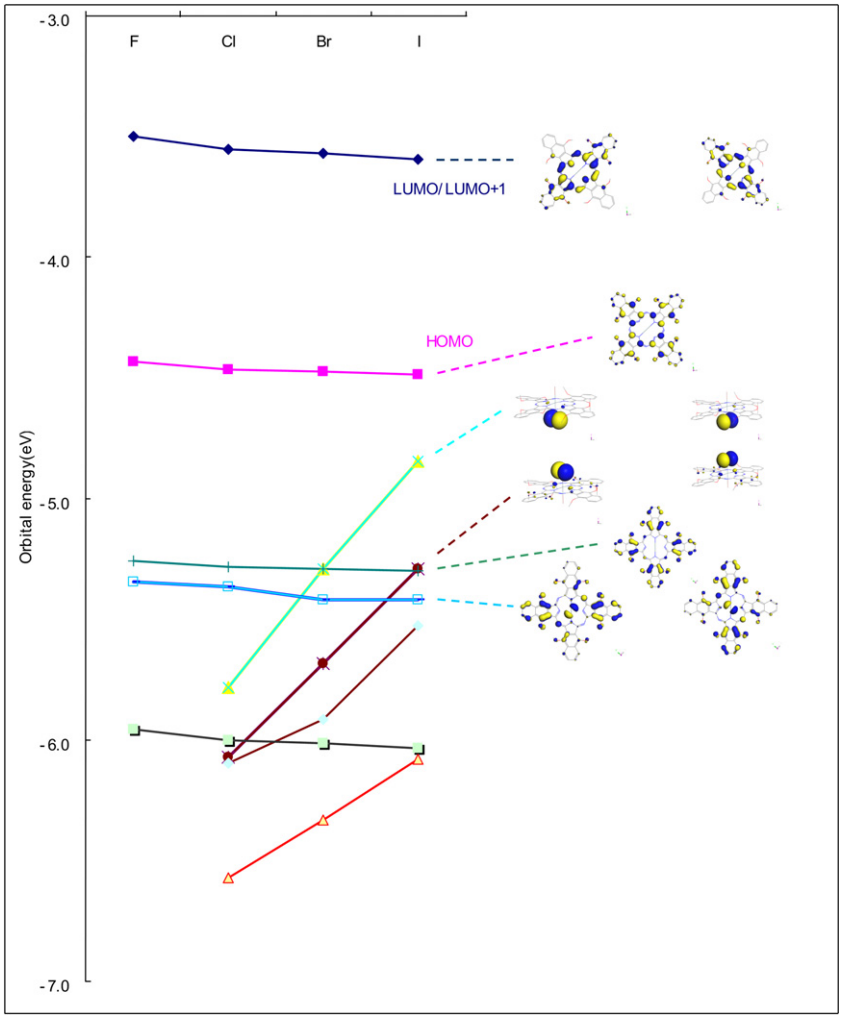

Fig. 6. The correlation diagram of the frontier molecular orbitals and their level ordering orbital energies for $SnNc(OBu)_8X_2$.

p_x and p_y orbitals. The bonding between Sn and the axial halogen ligands is described by the molecular orbitals whose main contribution is from the valence p_z orbitals of axial ligands and the Sn atom. As shown in Fig. 6, the energies of the molecular orbitals which are mainly contributed to by the naphthalocyanine ring, including the HOMO and LUMO, are slightly changed as the axial ligands change from F to I. As a result, the bonding between the Sn atom and the axial halogen ligands affects the structure of the naphthalocyanine ring and the shift of the Q-bands.

4. Conclusions

We have prepared and characterized a series of tin octabutoxy naphthalocyanines, which show near infrared absorption with a high extinction coefficient in the region 900–930 nm. The position of the Q-band in the series $SnNc(OBu)_8F_2$ (906 nm) to $SnNc(OBu)_8I_2$ (926 nm) is more red-shifted the heavier the halogen ligand. The tin naphthalocyanine with a heavy halide ligand becomes more concave, and the Sn–X bond is located at a longer distance out of the ring. The difference of the two axial bond lengths varies dramatically from 0.003 to 0.104 Å with the change of the axial ligands from F to I. The degree of the concave distortion is larger in the order $I > Br > Cl > F$, with the increase of atomic size and decrease of electronegativity. The transition dipole moment lies in the naphthalocyanine plane perpendicular to the permanent dipole moment in the tin–halide bond, which is related to the electronegativity of the axial halide. The energies of the molecular orbitals which are mainly contributed to by the naphthalocyanine ring, including the HOMO and LUMO, are slightly changed as the axial ligands change from F to I. As a result, the bonding between the Sn atom and the axial halogen ligands affects the structure of the naphthalocyanine ring and the shift of the Q-bands. The near-infrared absorption is further shifted to the infrared by the interaction with C_{60}. These tin halo naphthalocyanines could be a molecular engineering tool for spectral tuning in near infrared applications.

Appendix A. Supplementary material

Supplementary data associated with this article can be found, in the online version, at doi:10.1016/j.poly.2007.01.045.

References

[1] (a) A.B.P. Lever, Chemtech (1987) 506;
(b) R.O. Loutfy, A.M. Hor, G. DiPaola-Baranyi, C.K. Hsiao, J. Imaging Sci. 29 (1985) 116;
(c) N.J. Long, Angew. Chem., Int. Ed. Engl. 34 (1995) 21;
(d) M. Emmelius, G. Pawlowski, H.W. Vollmann, Angew. Chem., Int. Ed. Engl. 28 (1989) 1445;
(e) J. Fabian, H. Nakazumi, M. Matsuoka, Chem. Rev. (1992) 1197;
(f) J.W. Gregory, J.P. Sullivan, S.S. Wanis, N.M. Komerath, J. Acoust. Soc. Am. 119 (2006) 251.
[2] (a) M. Adachi, Y. Nagao, Chem. Mater. 11 (8) (1999) 2107;
(b) J. Fabian, H. Nakazumi, M. Matsuoka, Chem. Rev. 92 (1992) 1197;
(c) K.-Y. Law, Chem. Rev. 93 (1993) 449;
(d) S. Comby, D. Imbert, A.-S. Chauvin, J.-C. G. Bunzli, Inorg. Chem. 45 (2006) 732;
(e) K. McEwan, K. Lewis, G. Yang, L. Chng, Y. Lee, W. Lau, K. Lai, Adv. Funct. Mater. 13 (2003) 863;
(f) N.G. Pschirer, C. Kohl, F. Nolde, J. Qu, K. Mullen, Angew. Chem., Int. Ed. 45 (2006) 1401.
[3] (a) X. Huang, I.H. El-Sayed, W. Qian, M.A. El-Sayed, J. Am. Chem. Soc. 128 (2006) 2115;
(b) B. Xing, A. Khanamiryan, J. Rao, J. Am. Chem. Soc. 127 (2005) 4158.
[4] (a) R. Weissleder, C.H. Tung, U. Mahmood, A. Bogdanov, Nat. Biotech. 17 (1999) 375;
(b) A. Becker, C. Hessenius, K. Licha, B. Ebert, U. Sukowski, W. Semmler, B. Wiedenmann, C. Grotzinger, Nat. Biotech. 19 (2001) 327;
(c) S. Kim, Y.T. Lim, E.G. Soltesz, A.M. De Grand, J. Lee, A. Nakayama, J.A. Parker, T. Mihaljevic, R.G. Laurence, D.M. Dor, L.H. Cohn, M.G. Bawendi, J.V. Frangioni, Nat. Biotech. 22 (2004) 93;
(d) R. Weissleder, V. Ntziachristos, Nat. Med. 9 (2003) 123.
[5] (a) T.J. Dougherty, Photochem. Photobiol. 58 (1993) 895;
(b) T.J. Dougherty, Proc. SPIE IS 6 (1990) 1;
(c) J.C. Maziere, P. Morliere, R. Santus, J. Photochem. Photobiol. B: Biol. 8 (1991) 351;
(d) D. Phillips, Pure & Appl. Chem. 67 (1995) 117;
(e) S.I. Zaidi, R. Agarwal, G. Eichler, B.D. Rither, M.E. Kenney, H. Mukhtar, Photochem. Photobiol. 58 (1993) 204;
(f) M.W. Berns, Sci. Am. 1 (June) (1991) 84.
[6] (a) K. Mansour, J. Daniel Alvarez, K.J. Perry, I. Choong, S.R. Marder, J.W. Perry, Proc. SPIE 1853 (1993) 132;
(b) J.W. Perry, K. Mansour, S.R. Marder, C.-T. Chen, P. Miles, M.E. Kenney, G. Kwag, Mater. Res. Soc. Symp. Proc. 374 (1995) 257.
[7] (a) A.D. Becke, Phys. Rev. A88 (1988) 3098;
(b) C. Lee, W. Yang, R.G. Parr, Phys. Rev. B37 (1988) 785.
[8] M. Dolg, U. Wedig, H. Stoll, H. Preuss, J. Chem. Phys. 86 (1987) 866.
[9] (a) B. Delley, J. Chem. Phys. 92 (1990) 508;
(b) B. Delley, J. Chem. Phys. 113 (2000) 7756.
[10] Material Studio DMOL^3 User Guide, Accelrys Inc., San Diego, 2002.
[11] J. Ridley, M. Zerner, Theor. Chem. Acta 42 (1987) 347.
[12] T. Clark, A. Alex, B. Beck, F. Burkhardt, J. Chandrasekhar, P. Gedeck, A. Horn, M. Hutter, B. Martin, G. Rauhut, W. Sauer, T. Schindler, T. Steinke, VAMP, Version 8.0, Universitaẗ Erlangen, Erlangen, Germany, 2003, This version is provided as part of Materials Studio 4.0 by Accelrys Inc.
[13] B.D. Rihter, M.E. Kenney, W.E. Ford, M.A.J. Rodgers, J. Am. Chem. Soc. 115 (1993) 8146.
[14] (a) B.E. Mann, in: R.K. Harris, B.E. Mann (Eds.), Group IV-Silicon, Germanium, Tin and Lead, Academic, New York, 1978 (Chapter 4);
(b) D.P. Arnold, J.P. Bartly, Inorg. Chem. 33 (1994) 1486.
[15] R.K. Harris, J.D. Kennedy, W. McFarlane, in: R.K. Harris, B.E. Mann (Eds.), Group IV-Silicon, Germanium, Tin and Lead, Academic, New York, 1978 (Chapter 10).
[16] (a) P.D. Boyd, C.A. Reed, Acc. Chem. Res. 38 (2005) 235;
(b) D.M. Guldi, A. Gouloumis, P. Vazquez, T. Torres, V. Georgakilas, M. Prato, J. Am. Chem. Soc. 127 (2005) 5811;
(c) F. D'Souza, R. Chitta, S. Gadde, M.E. Zandler, A.L. McCarty, A.S.D. Sandanayaka, Y. Araki, O. Ito, J. Phys. Chem. A 110 (2006) 4338.